HHS Public Access

Author manuscript

Magn Reson Imaging. Author manuscript; available in PMC 2016 May 01.

Published in final edited form as:

Magn Reson Imaging. 2015 May ; 33(4): 437–447. doi:10.1016/j.mri.2014.12.008.

Evidence of Altered Age-Related Brain Cytoarchitecture in Mouse Models of Down syndrome: A Diffusional Kurtosis Imaging Study

Xingju Nie[1,2], **Eric D. Hamlett**[3], **Ann-Charlotte Granholm**[3], **Edward S. Hui**[4], **Joseph A. Helpern**[1,2,3], **Jens H. Jensen**[1,2], **Heather A. Boger**[3], **Heather R. Collins**[2], and **Maria F. Falangola**[1,2,3,*]

[1]Department of Radiology and Radiological Science, Medical University of South Carolina, Charleston, SC 29425

[2]Center for Biomedical Imaging, Medical University of South Carolina, Charleston, SC 29425

[3]Department of Neuroscience, Medical University of South Carolina, Charleston, SC 29425

[4]Department of Diagnostic Radiology, Li Ka Shing Faculty of Medicine, The University of Hong Kong, Pokfulam, Hong Kong SAR, China

Abstract

Mouse models of Down syndrome (DS) exhibit abnormal brain developmental and neurodegenerative changes similar to those seen in individuals with DS. Although DS mice have been well characterized cognitively and morphologically there are no prior reports utilizing diffusion MRI. In this study we investigated the ability of diffusional kurtosis imaging (DKI) to detect the progressive developmental and neurodegenerative changes in the Ts65Dn (TS) DS mouse model. TS mice displayed higher diffusional kurtosis (DK) in the frontal cortex (FC) compared to normal mice at 2 months of age. At 5 months of age, TS mice had lower radial kurtosis in the striatum (ST), which persisted in the 8-month-old mice. The TS mice exhibited lower DK metrics values in the dorsal hippocampus (HD) at all ages, and the group difference in this region was larger at 8-months. Regression analysis showed that normal mice had a significant age-related increase in DK metrics in FC, ST and HD. On the contrary, the TS mice lacked significant age-related increase in DK metrics in FC and ST. Although preliminary, these results demonstrate that DK metrics can detect TS brain developmental and neurodegenerative abnormalities.

Keywords

MRI; diffusion; kurtosis; DKI; Down syndrome; mouse

*Corresponding Author: Maria F. Falangola, M.D., Ph.D., Department of Radiology and Radiological Science, Center for Biomedical Imaging, MSC 120, Medical University of South Carolina, 68 President St, Bioengineering Building Rm 212, Charleston SC 29425-0120, falangol@musc.edu, Tel: 843.876.2466, Fax: 843.876.2469.

1. Introduction

Down syndrome (DS) is the most common genetic cause of intellectual disability in children. Additionally, most adults with DS will eventually show both clinical and neuropathologic hallmarks of Alzheimer's disease (AD) (1–4). Despite much research toward understanding the pathogenesis of cognitive dysfunction and neurodegeneration in DS, the biological mechanisms underlying these impairments are still poorly understood (3, 4). Due to a significantly improved average lifespan for DS individuals in the last couple of decades, the prevalence of DS-related dementia (DSD) has also increased significantly. Unfortunately, there are no effective therapeutic interventions that prevent AD-like pathology in young adult or middle-aged DS individuals. Based on the increased longevity of individuals with DS, there has been a recent surge in research efforts as well as a multi-institute research plan at the National Institutes of Health (NIH) in this area (http://nih.gov/news/health/oct2012/nichd-26.htm).

Several mouse models of DS (5–10) have been described and used to study the morphological abnormalities and the mechanisms underlying DS-associated cognitive disabilities. Among them, the Ts65Dn (TS) model carries trisomic segments of mouse chromosome 16 that contain regions orthologous to human chromosome 21, and share some DS-relevant behavioral and morphological features (11,12). The TS model has been widely used for the study of age-related neurodegeneration and cognitive impairments parallel to those seen in the brain of DS individuals (13, 14). These mice exhibit memory and learning deficits associated with progressive loss of basal forebrain cholinergic neurons (15–17) and reduced hippocampal long-term potentiation (LTP) and increased long-term depression (LTD) (18,19). Morphological abnormalities are seen in the dendritic and synaptic structure in the Ts65Dn and other mouse models of DS (20–24). In these studies, investigators reported widespread structural abnormalities in the hippocampus as well as in other brain regions, including enlargement of presynaptic boutons and dendritic spines. Moreover, a significant decrease in the density of dendritic spines and changes in the pattern of innervation of dentate granule cell neurons were observed. Our group and others have demonstrated significant deterioration of working and reference spatial memory, as well as frontal cortex-related working memory with age in these DS mouse models (25–27). We have also shown increased inflammatory markers, as well as age-related gliosis, especially in the limbic system compared to age-matched normosomic (control) mice (28–29).

Despite the fact that these DS mouse models have been well characterized cognitively and morphologically, little has been published using in vivo neuroimaging methods such as MRI. Chen et al. (30) reported decreased T_2 relaxation time in brain regions that receive cholinergic innervations in old (>12 months old) Ts65Dn mice, and Ishihara et al. (31) reported ventricular enlargement and impaired neurogenesis in the brains of Ts1Cje and Ts2Cje mouse models. Recently, Kaur et al. (32) reported reduced glutamate in the hippocampus of Ts2 mice measured by magnetic resonance spectroscopy (MRS), which was accompanied by reduced mRNA and protein levels of N-methyl-D-aspartate (NMDA) receptors (NMDA-R1). Similarly, Santin et al. (33) reported significantly lower levels of glutamine in the hippocampus of Ts65Dn using in vivo MRS. However, to our knowledge,

there have been no diffusion MRI (dMRI) studies reported in any mouse model of DS to date.

Diffusion MRI is a powerful method for probing brain microstructure abnormalities and has been extensively used to demonstrate changes with normal aging and in several neurological diseases (34,35), both in humans and animals. Diffusional kurtosis imaging (DKI) is a specific dMRI technique that extends diffusion tensor imaging (DTI) by quantifying the non-Gaussian behavior of water diffusion, contributing additional information beyond that provided by DTI (36–38). Aside from providing all of the diffusion indices conventionally obtained with DTI, DKI also provides the metrics of diffusional non-Gaussianity, such as mean (MK), axial ($K_{//}$) and radial ($K_{\perp}$) kurtoses. These additional metrics can further help in our understanding of normal and abnormal brain tissue cytoarchitecture. Albeit a relatively new method, DKI is already yielding promising preliminary results in studies of normal aging and other brain diseases (39–47). Furthermore, our own animal investigations, as well as studies from other groups, have shown that DK metrics are sensitive to changes in brain microstructural complexity that may be associated with brain development (48), aging (49), amyloid-beta (Aβ) deposition (50), and myelin abnormalities (51). Therefore, the goal of this study was to investigate the ability of DK metrics to detect the progressive abnormal developmental and neurodegenerative brain changes that have been well documented in mouse models of Down syndrome.

2. Methods

2.2 Animals

All experimental procedures were approved by the Institutional Animal Care and Use Committee at Medical University of South Carolina (MUSC) and in accordance with the National Institutes of Health (NIH) Guide for Care and Use of Laboratory Animals.

Ts65Dn (TS, $n = 8$) and age-matched normosomic littermates (NS, littermates, $n = 8$) male mice were studied longitudinally at 2, 5 and 8 months of age. Mice partially trisomic for a segment of murine chromosome 16 just proximal to the gene for App and extending to the gene for myxovirus resistance (Mx) were developed by M. Davisson at Jackson Laboratories (51). Controls for this experiment were normosomic littermates (NS) to the TS mice with the same genetic background (B6C3HF1). As the C3H mouse strain carries the retinal degeneration allele (rd), the TS and NS were screened and found free of retinal degeneration at Jackson Laboratories (Bar Harbor, ME) before shipment to MUSC. The trisomy is maintained by mating female carriers (the males are sterile) to C57Bl/6J×C3H/HeSnJ F1 males on a segregated genetic background (52). All mice were housed in temperature- and humidity-controlled rooms on a 12-h light/dark cycle (lights on at 6:00 AM) in an accredited animal care facility.

2.3 MRI data collection

Mice were anesthetized using an isoflurane vaporizer set at the following percentages: 3% for induction, 2% during pilot scanning, and 1.5% during data acquisition. An animal monitoring unit (SA instruments, Inc., model 1025, Stony Brook, NY) was used to record respiration and rectal temperature. Respiration was measured with a pressure transducer

placed under the abdomen just below the ribcage. Body temperature was maintained using ventilated warm air, controlled by a feedback circuit between the heater and thermistor. After induction, mice were placed on a holder and restrained using a bite bar and ear bars placed in the auditory canal. Oxygen was used as the carrier gas and delivered at a low flow rate (≤ 0.5 L/min) to a cone positioned before the bite bar, where gases mixed with air and passed over the rodent's nose. All animals were maintained at 37.0 ± 0.2 °C and respiration ranged between 50 and 70 breaths per minute with a median heart rate of 500 beats per minute during scanning.

The in vivo MRI experiments were performed on a 7T BioSpec 70/30 horizontal scanner (Bruker BioSpin, Ettlingen, Germany) at MUSC, equipped with a 12 cm inner diameter actively shielded gradient system (440 mT/m) with a quadrature volume coil (T128038) for signal transmission and a mouse brain array coil (T11765) for signal reception. A 2-shot spin-echo echo planar imaging (SE-EPI) sequence was used for DKI acquisition. Sequence parameters were: TR/TE=3750/32.6ms, δ/Δ=5/18ms, slice thickness=0.6 mm, 12 slices with no gap, data matrix=128×128, image resolution=156×156 μm^2, 2 averages, 64 gradient directions and 4 b-values for each gradient direction (0.5, 1, 1.5 and 2 ms/μm^2). Total acquisition time was approximately 35 minutes.

2.4 DKI post-processing and Image analysis

DKI post-processing for both data sets was performed using DKE software (53) (http://nitrc.org/projects/dke). Parametric maps were obtained by fitting dMRI signal measurements to the DKI signal model for each voxel using a linearly constrained weighted linear least squares fitting algorithm. Parametric maps of the conventional diffusion tensor (DT) metrics of mean (MD), axial ($D_{\parallel}$) and radial ($D_{\perp}$) diffusivities, as well as the additional DK metrics of MK, $K_{\parallel}$, and $K_{\perp}$ were subsequently computed. All of these metrics were estimated from the diffusion and diffusional kurtosis tensors (36, 37). MD corresponds to the diffusivity averaged over all diffusion directions, $D_{\parallel}$ corresponds to the diffusivity in the direction of the principal diffusion tensor eigenvector, and $D_{\perp}$ corresponds to the diffusivity averaged over all diffusion directions perpendicular to the principal diffusion tensor eigenvector. The additional metrics of MK, $K_{\parallel}$ and $K_{\perp}$, are kurtosis analogs of MD, $D_{\parallel}$ and $D_{\perp}$ that quantify the diffusional non-Gaussianity (36,37). It is worth noting that, due to the inclusion of non-Gaussian effects, the DKI-derived estimates of diffusivities will generally be more accurate than those obtained with DTI (54).

Multi-slice regions-of-interest (ROIs) were manually drawn on the b=0 image, using ImageJ (http://rsb.info.nih.gov/). Anatomical guidelines for outlining these regions were determined by comparing anatomical structures in the MRI slices with a standard mouse atlas (55). Although TS mice have brain shape differences relative to control mice, this does not alter the brain regional anatomical landmarks, and there were no statistical differences in the number of voxels for all ROIs between the 2 groups. The ROIs, comprising of frontal cortex (FC), cortex (CT), striatum (ST) and hippocampus (Total – HT; Dorsal – HD; Ventral – HV), are illustrated in Fig.1. FC included mainly cingulate cortex and CT included frontal, parietal and temporal cortex. The average regional value for each dMRI metric was obtained from the voxels within each ROI. To minimize the effect of cerebrospinal fluid (CSF)

contamination, all voxels with MD>1.5 μm2/ms were excluded from the ROIs prior to parameter quantification.

2.5 Statistical analysis

All data are expressed as group averaged means ± standard error of the mean (SEM). One-way analysis of variance (ANOVA) was performed to compare the mean of diffusion metrics between the two groups. An uncorrected p-value of ≤0.05 was considered to be statistically significant. Additionally, a Bonferroni correction was applied to explore which group differences would remain significant after correcting for multiple comparisons. Linear regression analysis was conducted to investigate the age-related effect on each diffusion metric, for each brain region in each group (TS and NS). We also determined whether the slopes of the age-trajectory lines were significantly different from each other taking into account the slope, standard error, and sample size; the t-value for the difference between the two slopes was determined as previously reported (56,57). A value of less than 0.05 indicated that the two slopes were significantly different. ANOVA and regression analyses were performed using SPSS version 20.0 (IBM SPSS Statistics for Windows, Version 20.0. Armonk, NY: IBM Corp).

3. Results

The anatomical images (Fig. 2) illustrated the phenotypic difference between the brains of TS and NS mice. Increase in the height and decrease in the rostrocaudal length of the cerebrum, and decrease in the mediolateral width of the posterior cerebrum, as previously described in this model (58), were apparent.

3.1 Group Analysis

Representative parametric maps of all diffusion metrics in a single slice of a normal control mouse brain are shown in Fig. 3. Estimates of the diffusion metrics (mean ± standard error of the mean (SEM)) in each brain ROI for each time point (2, 5 and 8 months of age) are presented in Tables 1–3. DT metrics showed no group differences in any of the brain ROIs examined, at any age. DK metrics showed significant differences between the two groups in several brain ROIs. In the FC, all DK metrics showed increased mean values in 2-month old TS mice compared to NS mice. No changes in DK metrics were detected in FC in 5-month old TS mice. In 8-month old TS mice, MK and $K_{\parallel}$ were decreased in the FC; although $K_{\perp}$ showed a trend for decrease it did not reach statistical significance, which may be due to the fact that the number of TS mice at this age was reduced to only 4. We observed an unexpected high mortality in the TS group; at 5 months only 5 out of 8 TS mice survived, and by 8 months only 4 out of the 8 initial TS mice had survived. In the CT, no changes in DK metrics were observed in both 2- and 5-month old TS mice, but 8-month old TS mice showed a significant decrease in $K_{\perp}$ compared to NS mice. There was a decrease in $K_{\perp}$ in the ST in 5-month old TS mice followed by a decrease in $K_{\parallel}$ and $K_{\perp}$ when TS mice reached 8 months of age. In the hippocampus, TS mice exhibited lower values for all DK metrics at all ages in the HD, and the group difference in this region was larger at 8-months. HV showed only trends for decrease in MK and $K_{\perp}$ but these did not reach statistical significance. HT showed significant decrease in MK and $K_{\perp}$ in 8-month old TS mice.

3.2 Age-related trajectories

Linear regression analysis was performed to identify age-related changes for each diffusion metric in each each group (Figs. 4–6). There was no significant relationship between DT metrics and age in FC, HD, HV and HT for both NS and TS groups, except for $D_{\perp}$ in the HD of the NS group. In the ST, both MD and $D_{\parallel}$ displayed significant increase with age for the NS group with no change in the TS group. On the contrary, DK metrics increased significantly with age in NS mice in all ROIs examined, except for $K_{\parallel}$ which did not show significant increase with age in the HV (data not shown). In contrast, DK metrics did not change significantly with age in TS mice, except for $K_{\parallel}$ in the HD which did significantly increase with age. When considering the whole cortex (CT), both DT and DK metrics did significantly increase with age in both NS and TS groups.

The slopes of the age-trajectory lines were significantly different for all DK metrics (MK, $K_{\parallel}$ and $K_{\perp}$,) in the FC, for MK and $K_{\perp}$ in the ST and for MK and $K_{\parallel}$ in the HD (Figs. 4–6). TS mice had higher MK, $K_{\parallel}$ and $K_{\perp}$ in the FC compared with NS at 2 months and did not change significantly through 8 months of age. In NS mice, all DK metrics (MK, $K_{\parallel}$ and $K_{\perp}$) increased significantly with age in the FC. In the striatum, NS and TS mice had similar DK metrics at 2 months, and NS mice showed significant age-related increase in MK and $K_{\perp}$, but no significant change with age was observed for the TS mice. TS mice had lower MK, $K_{\parallel}$ and $K_{\perp}$ in the HD compared with NS at 2 months, and despite the DK metrics increase with age for both groups, the slopes of the age-trajectory lines were statistically different for MK and $K_{\parallel}$. There were no differences between the age-trajectory slopes for DK metrics in CT, HV and HT, and for all DT metrics in all brain regions examined.

4. Discussion

The interpretation of changes in diffusion MRI metrics is complex. Unlike DTI, DKI enables the degree of diffusional non-Gaussianity to be quantified, and may more accurately reflect the complexity and heterogeneity of the tissue’s microenvironment. DK tends to increase with diffusional heterogeneity and can be altered by water exchange or by diffusion barriers.

The present data show group (NS vs. TS) and age-related differences in diffusion metrics, possibly reflecting the brain’s developmental and neurodegenerative abnormalities previously described in mouse models of DS (11–14, 59). The morphological changes that occur during normal brain development and maturation, which are well described in the literature (60–62), lead to significant changes in cortical growth and myelination. Our dMRI results appear to capture an increase in brain microstructural complexity with age in normal mice, as reflected by increase in DK metrics in several brain regions, as previously reported in a rodent brain maturation study (48). Additionally, the brain developmental and age-related changes that are associated with brain defects in DS, such as altered neurogenesis, hypocellularity, altered synaptic development and neurodegeneration have been well documented in DS mouse models (20–24, 59). Our results appear to capture these developmental and neurodegenerative abnormalities, as reflected by the absence of significant changes in DK metrics with age and lower DK values in the hippocampus of these mice.

Our results indicate that DK can detect early developmental abnormalities in the prefrontal cortex (FC) and hippocampus (HD) of 2-month old TS mice. These mice showed higher DK values in FC and lower DK values in dorsal hippocampus compared with NS mice at this age (Table 1). The increased kurtosis values in the frontal cortex of 2-month old TS mice could conceivably reflect increased diffusional heterogeneity due to the abnormal cortical lamination, less coherence in neurite orientations and smaller, less branched and less spinous dendrites as previously described in this region (20,63)". The lower DK values in the dorsal hippocampus of TS mice at this age may be related to both the defects in axonal spread and enlargements of dendritic spines, causing diffusion dead-space microdomains (21–24), as well as abnormal myelination of the hippocampus formation, as has been described in humans (64). At 5 months of age, TS mice showed lower $K_{\perp}$ values in the striatum (ST; Table 2), which may also be related to abnormality in the myelination process. In this model, impaired corticostriatal transmission and plasticity has been described, where loss of LTP in striatal cholinergic interneurons of 6-month old TS mice is accompanied by a severe impairment of endogenous cholinergic signaling within the striatum (65). These ST and HD changes continue to be present until 8 months of age.

Since there is no quantitative study of the myelination process in any of the mouse models of DS, we can only speculate, based on human post-mortem studies, about the possible morphological correlates of our dMRI results. In humans, a myelination delay has been reported affecting tracks with late and slow cycle of myelination, such as associated and intercortical fibers of the frontal-temporal connections (66). Also, previous reports in humans (64) showed that the sequence of myelination in hippocampus formation of both DS and controls are similar, but the number of myelinated fibers and their density are lower in DS when compared to age-matched controls. Interestingly, this difference between the density of myelinated fibers of DS patients and controls is mild in the first few months after birth, but increases and becomes more evident at older ages. Other possible explanations are the additional morphological abnormalities described in the hippocampus of the TS mice, such as lower neuronal density in CA1 and fewer granule cells in the dentate gyrus with small spine density.

In 8-month old TS mice, DK metrics were decreased compared with NS mice in the FC, representing a lack of brain maturation in this region. Indeed, the DK metrics in the FC of NS mice increased significantly with age whereas they did not change significantly with age in TS mice (Figure 4). In the HD, despite the fact that both groups showed increases in DK metrics with age, the slopes of the age-trajectory lines were statistically different for MK and $K_{\parallel}$, but at all age time points TS mice had smaller DK values compared with NS mice. The DK changes present in the hippocampus at later ages (5 to 8 months of age), when cognitive defects start to manifest in TS mice (26), may be associated with neurodegenerative changes related to neuroinflammation, increased oxidative stress, and the development of AD-like neuropathology with cholinergic neuron degeneration and age-related increased in APP and β-amyloid levels as previously described in this model (14–17).

Although these are preliminary results with a limited number of mice, they seem to demonstrate that DK can detect early developmental abnormalities (frontal cortex, striatum

and hippocampus), which are part of the abnormal circuitry development (15), and may be associated with the cognitive defects seen in these DS mouse models that start around 5 months of age (26). The abnormal morphological changes in frontal cortex maybe driving the abnormalities in the myelination process in the striatum and causing defects in axonal projections into the dorsal hippocampus. This study therefore provides insight into the diffusion patterns of the cerebral microenvironment that are associated with genetically derived brain morphological abnormalities in the neural maturation and with the neurodegenerative process in DS.

Our study has important limitations. First, the relatively small number of TS mice at later age time points (5 and 8 months old) reduced the statistical power of the data analysis; therefore, these results should be cautiously interpreted. Although we do not know at this time the reason for this high mortality in the TS group, we speculate that a possible anesthetic sensitivity related to the successive imaging procedure could have altered the lifespan of these mice in the setting of a genetic vulnerability. Indeed, individuals with DS have been reported to respond differently to general anesthesia (67), so it is not unlikely that this also is true for the DS mouse models. Additionally, it has been reported that isoflurane exposure may lead to neurotoxicity and adverse effects in other mouse models, such as mouse models of Aβ deposition and tauopathy (68, 69). Another limitation is that our study lacks a direct correlation with behavior or morphology data. However, these DS mouse models have been well characterized cognitively and morphologically, by our group and others (20–28), and our discussion is based on the results of those previous detailed studies. Nevertheless, future studies with morphological correlations at each time point and applying advanced tissue modeling will address this limitation. We are currently developing tissue modeling methods for investigating the complex microarchitecture of grey matter (70). We also recognize that these results should be confirmed in a future study with a larger sample size and behavioral correlations.

5. Conclusion

The current in vivo dMRI study of a mouse model of DS demonstrates that DK metrics are sensitive indicators of changes in the complexity of the neurite architecture, and may be used as an in vivo biomarker for monitoring abnormal brain development, maturation and neurodegeneration in these mouse models. These results may also assist in the interpretation of results from future translational DKI studies related to human brain microstructure abnormalities in DS.

Acknowledgments

The authors wish to acknowledge and thank Ms. Claudia Umphlet and Mr. Alfred Moore for technical assistance.

This work was supported in part by research grants from NIA RO1 AG012122 and Alzheimer Association (DSADIIP-13-284845) (ACG).

References

1. Tyrrell J, Cosgrave M, McCarron M, McPherson J, Calvert J, Kelly A, McLaughlin M, Gill M, Lawlor BA. Dementia in people with Down's syndrome. Int J Geriatr Psychiatry. 2001; 16(12): 1168–74. [PubMed: 11748777]
2. Lott IT, Head E. Down syndrome and Alzheimer's disease: a link between development and aging. Ment Retard Dev Disabil Res Rev. 2001; 7(3):172–178. [PubMed: 11553933]
3. Albert MS. Parallels between Down syndrome dementia and Alzheimer's disease. Prog Clin Biol Res. 1992; 379:77–102. [PubMed: 1409754]
4. Bakkar, Rania M.; Luo, Guangju; Webb, Thomas A.; Crutcher, Keith A.; de Courten-Myers, Gabrielle M. (2010) Down's Syndrome with Alzheimer's Disease-Like Pathology: What Can It Teach Us about the Amyloid Cascade Hypothesis? International Journal of Alzheimer's Disease. 2010 Article ID 175818. 10.4061/2010/175818
5. Davisson MT, Schmidt C, Reeves RH, Irving NG, Akeson EC, Harris BS, Bronson RT. Segmental trisomy as a mouse model for Down syndrome. Prog Clin Biol Res. 1993; 384:117–133. [PubMed: 8115398]
6. Reeves RH, Irving NG, Moran TH, Wohn A, Kitt C, Sisodia SS, Schmidt C, Bronson RT, Davisson MT. A mouse model for Down syndrome exhibits learning and behavior deficits. Nat Genet. 1995; 11:177–184. [PubMed: 7550346]
7. Sérégaza Z, Roubertoux PL, Jamon M, Soumireu-Mourat B. Mouse models of cognitive disorders in trisomy 21: a review. Behav Genet. 2006; 36(3):387–404. [PubMed: 16523244]
8. Roubertoux PL, Carlier M. Mouse models of cognitive disabilities in trisomy 21 (Down syndrome). Am J Med Genet C Semin Med Genet. 2010; 154C(4):400–16. Review. [PubMed: 20981769]
9. Das I, Reeves RH. The use of mouse models to understand and improve cognitive deficits in Down syndrome. Disease Models & Mechanisms. 2011; 4:596–606. [PubMed: 21816951]
10. Liu C, Belichenko PV, Zhang L, Fu D, Kleschevnikov AM, Baldini A, Antonarakis SE, Mobley WC, Yu YE. Mouse Models for Down Syndrome-Associated Developmental Cognitive Disabilities. Dev Neurosci. 2011; 33(5):404–13. [PubMed: 21865664]
11. Holtzman DM, Santucci D, Kilbridge J, Chua-Couzens J, Fontana DJ, Daniels SE, Johnson RM, Chen K, Sun Y, Carlson E, Alleva E, Epstein CJ, Mobley WC. Developmental abnormalities and age-related neurodegeneration in a mouse model of Down syndrome. Proc Natl Acad Sci U S A. 1996; 93(23):13333–8. [PubMed: 8917591]
12. Villar AJ, Belichenko PV, Gillespie AM, Kozy HM, Mobley WC, Epstein CJ. Identification and characterization of a new Down syndrome model, Ts[Rb(12.1716)]2Cje, resulting from a spontaneous Robertsonian fusion between T(171)65Dn and mouse chromosome 12. Mamm Genome. 2005; 16(2):79–90. [PubMed: 15859352]
13. Hyde LA, Crnic LS. Age-related deficits in context discrimination learning in Ts65Dn mice that model Down syndrome and Alzheimer's disease. Behav Neurosci. 2001; 115(6):1239–1246. [PubMed: 11770055]
14. Lockrow JP, Fortress AM, Granholm AC. Age-related neurodegeneration and memory loss in down syndrome. Curr Gerontol Geriatr Res. 2012; 2012:463909.10.1155/2012/463909 [PubMed: 22545043]
15. Gotti S, Caricati E, Panzica G. Alterations of brain circuits in Down syndrome murine models. J Chem Neuroanat. 2011; 42(4):317–26. [PubMed: 21946025]
16. Seo H, Isacson O. Abnormal APP, cholinergic and cognitive function in Ts65Dn Down's model mice. Exp Neurol. 2005; 193(2):469–480. [PubMed: 15869949]
17. Lockrow J, Prakasam A, Huang P, Bimonte-Nelson H, Sambamurti K, Granholm AC. Cholinergic degeneration and memory loss delayed by vitamin E in a Down syndrome mouse model. Exp Neurol. 2009; 216:278–289. [PubMed: 19135442]
18. Siarey RJ, Stoll J, Rapoport SI, Galdzicki Z. Altered long-term potentiation in the young and old Ts65Dn mouse, a model for Down Syndrome. Neuropharmacology. 1997; 36(11–12):1549–54. [PubMed: 9517425]

19. Costa AC, Grybko MJ. Deficits in hippocampal CA1 LTP induced by TBS but not HFS in the Ts65Dn mouse: a model of Down syndrome. Neurosci Lett. 2005; 382:317–322. [PubMed: 15925111]
20. Dierssen M, Benavides-Piccione R, Martínez-Cué C, Estivill X, Florez J, Elston GN, DeFelipe J. Alterations of neocortical pyramidal cell pheno-type in theTs65Dn mouse model of Down syndrome:effects of environmental enrichment. Cereb Cortex. 2003; 13:758–764. [PubMed: 12816891]
21. Belichenko PV, Masliah E, Kleschevnikov AM, Villar AJ, Epstein CJ, Salehi A, Mobley WC. Synaptic structural abnormalities in the Ts65Dn mouse model of Down Syndrome. J Comp Neurol. 2004; 480(3):281–98. [PubMed: 15515178]
22. Belichenko PV, Kleschevnikov AM, Salehi A, Epstein CJ, Mobley WC. Synaptic and cognitive abnormalities in mouse models of Down syndrome: exploring genotype-phenotype relationships. J Comp Neurol. 2007; 504(4):329–45. [PubMed: 17663443]
23. Popov VI, Kleschevnikov AM, Klimenko OA, Stewart MG, Belichenko PV. Three-dimensional synaptic ultrastructure in the dentate gyrus and hippocampal area CA3 in the Ts65Dn mouse model of Down syndrome. J Comp Neurol. 2011; 519(7):1338–54. [PubMed: 21452200]
24. Benavides-Piccione R, Ballesteros-Yáñez I, de Lagrán MM, Elston G, Estivill X, Fillat C, Defelipe J, Dierssen M. On dendrites in Down syndrome and DS murine models: a spiny way to learn. Prog Neurobiol. 2004; 74(2):111–26. Review. [PubMed: 15518956]
25. Escorihuela RM, Vallina IF, Martínez-Cué C, Baamonde C, Dierssen M, Tobeña A, Flórez J, Fernández-Teruel A. Impaired short- and long-term memory in Ts65Dn mice, a model for Down syndrome. Neurosci Lett. 1998; 247(2–3):171–4. [PubMed: 9655620]
26. Hunter CL, Bimonte HA, Granholm AC. Behavioral comparison of 4 and 6 month-old Ts65Dn mice: age-related impairments in working and reference memory. Behav Brain Res. 2003; 138(2): 121–31. [PubMed: 12527443]
27. Granholm AC, Sanders LA, Crnic LS. Loss of cholinergic phenotype in basal forebrain coincides with cognitive decline in a mouse model of Down's syndrome. Exp Neurol. 2000; 161(2):647–63. [PubMed: 10686084]
28. Bimonte-Nelson HA, Hunter CL, Nelson ME, Granholm AC. Frontal cortex BDNF levels correlate with working memory in an animal model of Down syndrome. Behav Brain Res. 2003; 139(1–2): 47–57. [PubMed: 12642175]
29. Wilcock DM, Griffin WS. Down's syndrome, neuroinflammation, and Alzheimer neuropathogenesis. J Neuroinflammation. 2013; 10:84.10.1186/1742-2094-10-84 [PubMed: 23866266]
30. Chen Y, Dyakin VV, Branch CA, Ardekani B, Yang D, Guilfoyle DN, Peterson J, Peterhoff C, Ginsberg SD, Cataldo AM, Nixon RA. In vivo MRI identifies cholinergic circuitry deficits in a Down syndrome model. Neurobiol Aging. 2009; 30(9):1453–65. [PubMed: 18180075]
31. Ishihara K, Amano K, Takaki E, Shimohata A, Sago H, Epstein CJ, Yamakawa K. Enlarged brain ventricles and impaired neurogenesis in the Ts1Cje and Ts2Cje mouse models of Down syndrome. Cereb Cortex. 2010; 20(5):1131–43. [PubMed: 19710359]
32. Kaur G, Sharma A, Xu W, Gerum S, Alldred MJ, Subbanna S, Basavarajappa BS, Pawlik M, Ohno M, Ginsberg SD, Wilson DA, Guilfoyle DN, Levy E. Glutamatergic transmission aberration: a major cause of behavioral deficits in a murine model of Down's syndrome. J Neurosci. 2014; 34(15):5099–106. [PubMed: 24719089]
33. Santin MD, Valabrègue R, Rivals I, Pénager R, Paquin R, Dauphinot L, Albac C, Delatour B, Potier MC. In vivo (1) H MRS study in microlitre voxels in the hippocampus of a mouse model of Down syndrome at 11.7 T. NMR Biomed. 2014 Aug 1. [Epub ahead of print] PubMed. 10.1002/nbm.3155
34. Abe O, Aoki S, Hayashi N, Yamada H, Kunimatsu A, Mori H, Yoshikawa T, Okubo T, Ohtomo K. Normal aging in the central nervous system: quantitative MR diffusion-tensor analysis. Neurobiol Aging. 2002; 23(3):433–41. [PubMed: 11959406]
35. Stebbins GT, Murphy CM. Diffusion tensor imaging in Alzheimer's disease and mild cognitive impairment. Behav Neurol. 2009; 21(1):39–49. Review. [PubMed: 19847044]

36. Jensen JH, Helpern JA, Ramani A, Lu H, Kaczynski K. Diffusional Kurtosis Imaging: The Quantification of Non-Gaussian Water Diffusion by Means of MRI. Magn Reson Med. 2005; 53:1432–1440. [PubMed: 15906300]
37. Lu H, Jensen JH, Ramani A, Helpern JA. Three-dimensional characterization of non-gaussian water diffusion in humans using diffusion kurtosis imaging. NMR Biomed. 2006; 19(2):236–247. [PubMed: 16521095]
38. Jensen JH, Helpern JA. MRI quantification of non-Gaussian water diffusion by kurtosis analysis. NMR Biomed. 2010; 23(7):698–710. [PubMed: 20632416]
39. Falangola MF, Jensen JH, Babb JS, Hu C, Castellanos FX, Di Martino A, Ferris SH, Helpern JA. Age-related non-Gaussian diffusion patterns in the prefrontal brain. J MagnReson Imaging. 2008; 28(6):1345–50.
40. Helpern JA, Adisetiyo V, Falangola MF, Hu C, Di Martino A, Williams K, et al. Preliminary evidence of altered gray and white matter microstructural development in the frontal lobe of adolescents with attention-deficit hyperactivity disorder: a diffusional kurtosis imaging study. J Magn Reson Imaging. 2011; 33(1):17–23. [PubMed: 21182116]
41. Jensen JH, Falangola MF, Hu C, Tabesh A, Rapalino O, Lo C, et al. Preliminary observations of increased diffusional kurtosis in human brain following recent cerebral infarction. NMR Biomed. 2011; 24(5):452–7. [PubMed: 20960579]
42. Hui ES, Fieremans E, Jensen JH, Tabesh A, Feng W, Bonilha L, Spampinato MV, Adams R, Helpern JA. Stroke assessment with diffusional kurtosis imaging. Stroke. 2012; 43(11):2968–73. [PubMed: 22933581]
43. Van Cauter S, Veraart J, Sijbers J, Peeters RR, Himmelreich U, De Keyzer F, Van Gool SW, Van Calenbergh F, De Vleeschouwer S, Van Hecke W, Sunaert S. Gliomas: Diffusion Kurtosis MR Imaging in Grading. Radiology. 2012; 263(2):492–501. [PubMed: 22403168]
44. Grossman EJ, Ge Y, Jensen JH, Babb JS, Miles L, Reaume J, et al. Thalamus and Cognitive Impairment in Mild Traumatic Brain Injury: A Diffusional Kurtosis Imaging Study. Journal of Neurotrauma. 2011; 29(13):2318–27. [PubMed: 21639753]
45. Falangola MF, Jensen JH, Tabesh A, Hu C, Deardorff RL, Babb JS, Ferris S, Helpern JA. Non-Gaussian diffusion MRI assessment of brain microstructure in mild cognitive impairment and Alzheimer's disease. Magn Reson Imaging. 2013; 31(6):840–6. [PubMed: 23602730]
46. Coutu JP, Chen JJ, Rosas HD, Salat DH. Non-Gaussian water diffusion in aging white matter. Neurobiol Aging. 2014; 35(6):1412–21. [PubMed: 24378085]
47. Gong NJ, Wong CS, Chan CC, Leung LM, Chu YC. Aging in deep gray matter and white matter revealed by diffusional kurtosis imaging. Neurobiol Aging. 2014; 35(10):2203–16. [PubMed: 24910392]
48. Cheung MM, Hui ES, Chan KC, Helpern JA, Qi L, Wu EX. Does diffusion kurtosis imaging lead to better neural tissue characterization? A rodent brain maturation study. Neuroimage. 2009; 45(2): 386–92. [PubMed: 19150655]
49. Falangola MF, Guilfoyle D, Hui ES, Hu C, Gerum S, LaFrancois J, Nie X, Jensen JH, Tabesh A, Helpern JA. Diffusional Kurtosis Imaging Detects Age-related Grey matter Changes in the Normal Mouse Brain. Proc Intl Soc Mag Reson Med. 2012; 20:1241.
50. Vanhoutte G, Pereson S, Delgado Y, Palacios R, Guns PJ, Asselbergh B, Veraart J, Sijbers J, Verhoye M, Van Broeckhoven C, Van der Linden A. Diffusion kurtosis imaging to detect amyloidosis in an APP/PS1 mouse model for Alzheimer's disease. Magn Reson Med. 2013; 69(4): 1115–21. [PubMed: 23494926]
51. Falangola MF, Guilfoyle DN, Tabesh A, Hui ES, Nie X, Jensen JH, Gerum SV, Hu C, LaFrancois J, Collins HR, Helpern JA. Histological correlation of diffusional kurtosis and white matter modeling metrics in cuprizone-induced corpus callosum demyelination. NMR Biomed. 2014 Jun 3. [Epub ahead of print] PubMed. 10.1002/nbm.3140
52. Davisson MT, Schmidt C, Akeson EC. Segmental trisomy of murine chromosome 16: a new model system for studying Down syndrome. Prog Clin Biol Res. 1990; 360:263–80. [PubMed: 2147289]
53. Tabesh A, Jensen JH, Ardekani BA, Helpern JA. Estimation of tensors and tensor-derived measures in diffusional kurtosis imaging. Magn Reson Med. 2011; 65(3):823–36. [PubMed: 21337412]

54. Veraart J, Poot DHJ, Van Hecke W, et al. More accurate estimation of diffusion tensor parameters using diffusion Kurtosis imaging. Magn Reson Med. 2011; 65(1):138–145. [PubMed: 20878760]
55. Paxinos, G.; Franklin, K. The Mouse Brain in Stereotaxic Coordinates: Compact. 2. Academic; San Diego: 2003.
56. Cohen, J.; Cohen, P.; West, SG.; Aiken, LS. Applied Multiple Regression/Correlation Analysis for the Behavioral Sciences. 3. Mahwah, NJ: Lawrence; 2003.
57. Soper, DS. Significance of the Difference between Two Slopes Calculator [Software]. 2014. Available from http://www.danielsoper.com/statcalc
58. Aldridge K, Reeves RH, Olson LE, Richtsmeier JT. Differential effects of trisomy on brain shape and volume in related aneuploid mouse models. Am J Med Genet A. 2007; 143A(10):1060–70. [PubMed: 17431903]
59. Fillat C, Dierssen M, de Lagrán MM, Altafaj X. Insights from mouse models to understand neurodegeneration in Down syndrome. CNS Neurol Disord Drug Targets. 2010; 9(4):429–38. Review. [PubMed: 20522013]
60. Goffinet, Andre M.; Rakic, Pasko. Mouse Brain Development. Springer; Berlin Heidelberg: 2000.
61. Hedley-Whyte ET, Kirschner DA. Morphological evidence of alteration in myelinstructure with maturation. Brain Res. 1976; 113(3):487–97. [PubMed: 953750]
62. deToledo-Morrell L, Geinisman Y, Morrell F. Age-dependent alterations in hippocampal synaptic plasticity: relation to memory disorders. Neurobiol Aging. 1988; 9(5–6):581–90. Review. [PubMed: 3062469]
63. Haydar TF, Reeves RH. Trisomy 21 and early brain development. Trends Neurosci. 2012; 35(2): 81–91. Review. [PubMed: 22169531]
64. Ábrahám H, Vincze A, Veszprémi B, Kravják A, Gömöri É, Kovács GG, Seress L. Impaired myelination of the human hippocampal formation in Down syndrome. Int J Dev Neurosci. 2012; 30(2):147–58. [PubMed: 22155002]
65. Di Filippo M, Tozzi A, Ghiglieri V, Picconi B, Costa C, Cipriani S, Tantucci M, Belcastro V, Calabresi P. Impaired plasticity at specific subset of striatal synapses in the Ts65Dn mouse model of Down syndrome. Biol Psychiatry. 2010; 67(7):666–71. [PubMed: 19818432]
66. Wisniewski KE, Schmidt-Sidor B. Postnatal delay of myelin formation in brains from Down syndrome infants and children. Clin Neuropathol. 1989; 8(2):55–62. [PubMed: 2524302]
67. Meitzner MC, Skurnowicz JA. Anesthetic considerations for patients with Down syndrome. AANA J. 2005; 73(2):103–7. Review. [PubMed: 15835829]
68. Tang JX, Eckenhoff MF. Anesthetic effects in Alzheimer transgenic mouse models. Prog Neuropsychopharmacol Biol Psychiatry. 2013; 47:167–71. [PubMed: 22705294]
69. Menuet C, Borghgraef P, Voituron N, Gestreau C, Gielis L, Devijver H, Dutschmann M, Van Leuven F, Hilaire G. Isoflurane anesthesia precipitates tauopathy and upper airways dysfunction in pre-symptomatic Tau.P301L mice: possible implication for neurodegenerative diseases. Neurobiol Dis. 2012; 46(1):234–43. [PubMed: 22316605]
70. Hui ES, Glenn GR, Helpern JA, Jens JH. Kurtosis Analysis of Neural Diffusion Organization. Neuroimage. 2014 in press.

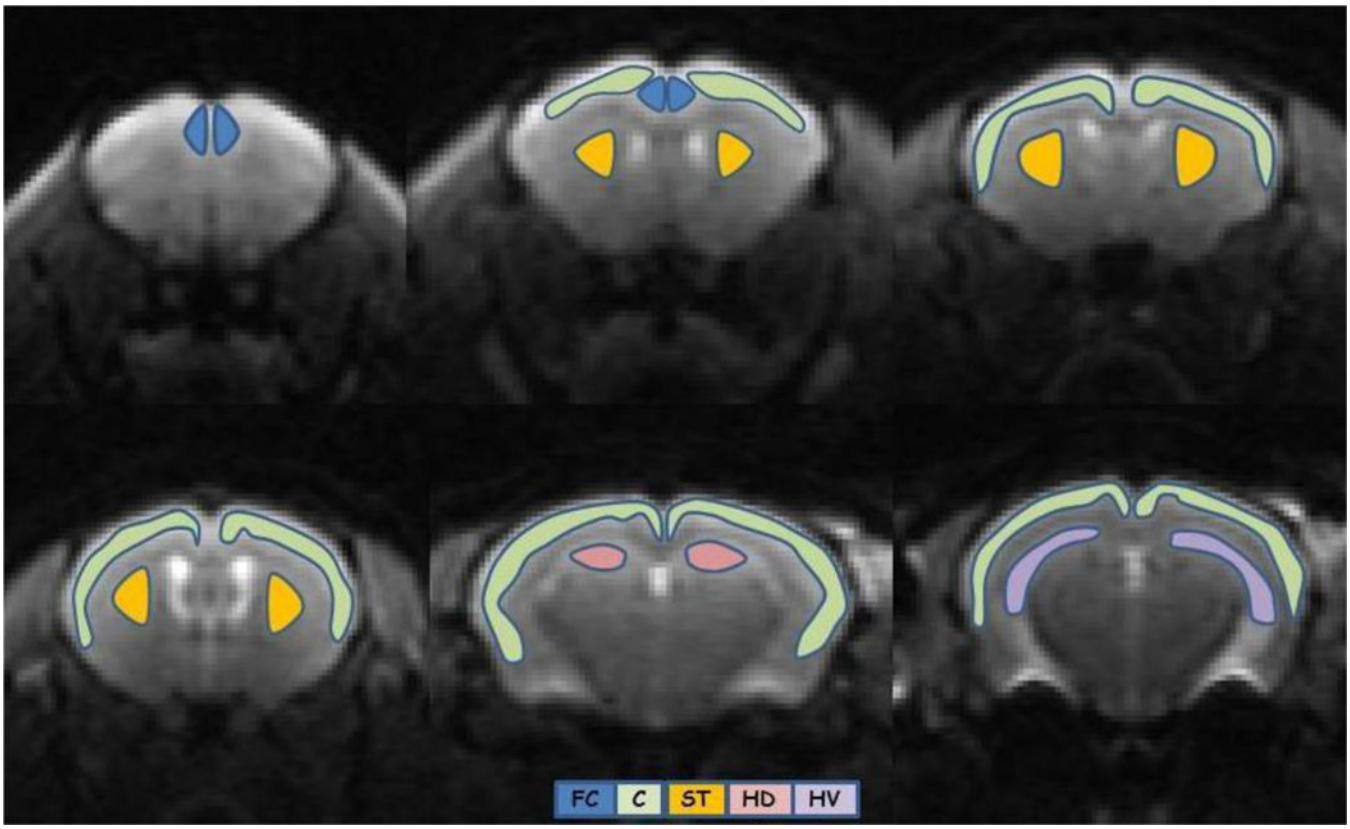

Figure 1.
Brain regions of interest: Frontal cortex (FC – blue), cortex (C – green), striatum (ST – orange) and hippocampus (dorsal (HD) – pink; ventral (HV) – purple).

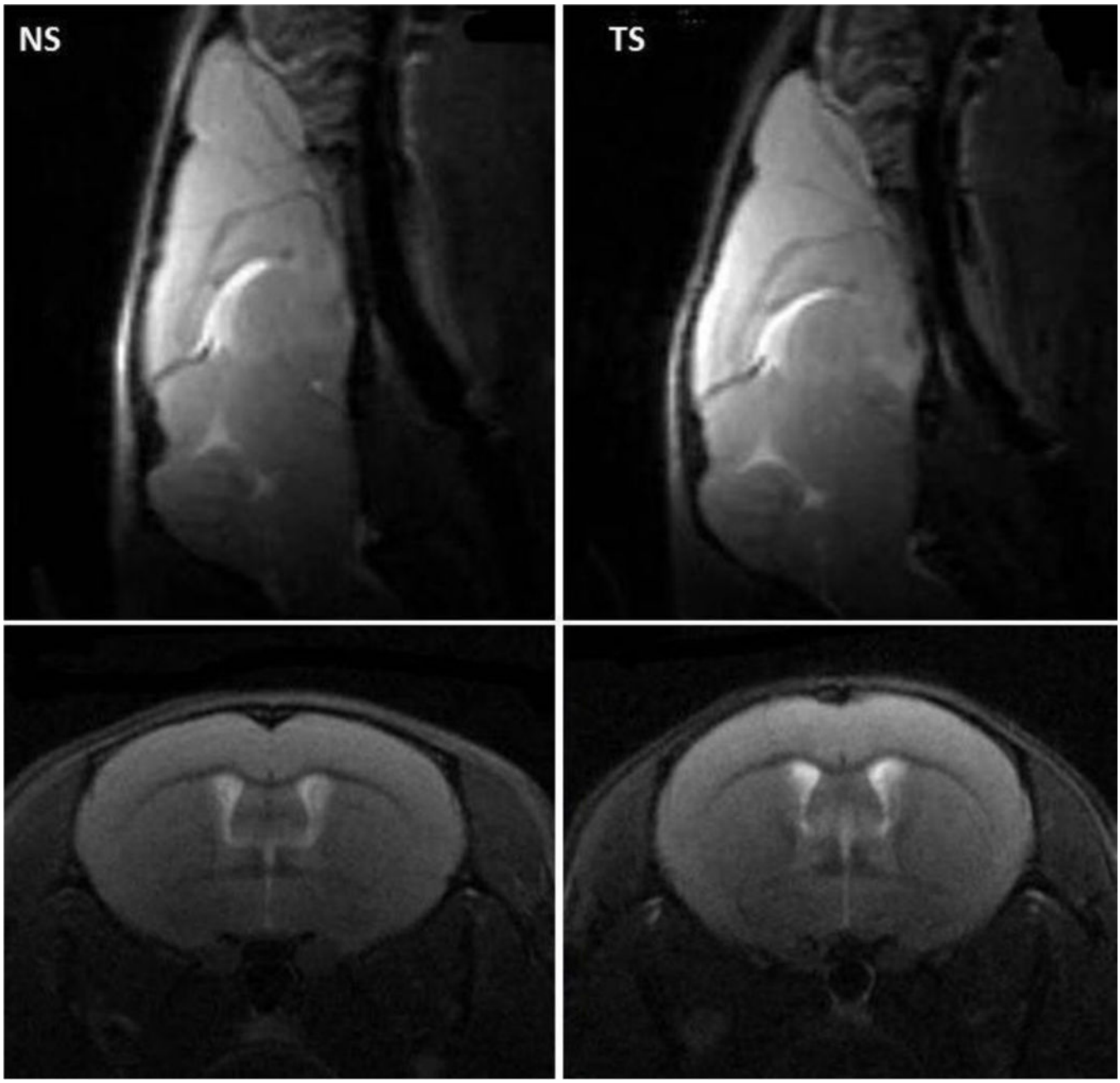

Figure 2.

Sagittal and coronal anatomical MRI showing the phenotypic difference between the brains of the Ts65Dn (TS) and normossomic control (NS). Note the increase of the cerebrum height and decrease of the rostrocaudal length of the cerebrum and mediolateral width of the posterior cerebrum in the TS mice.

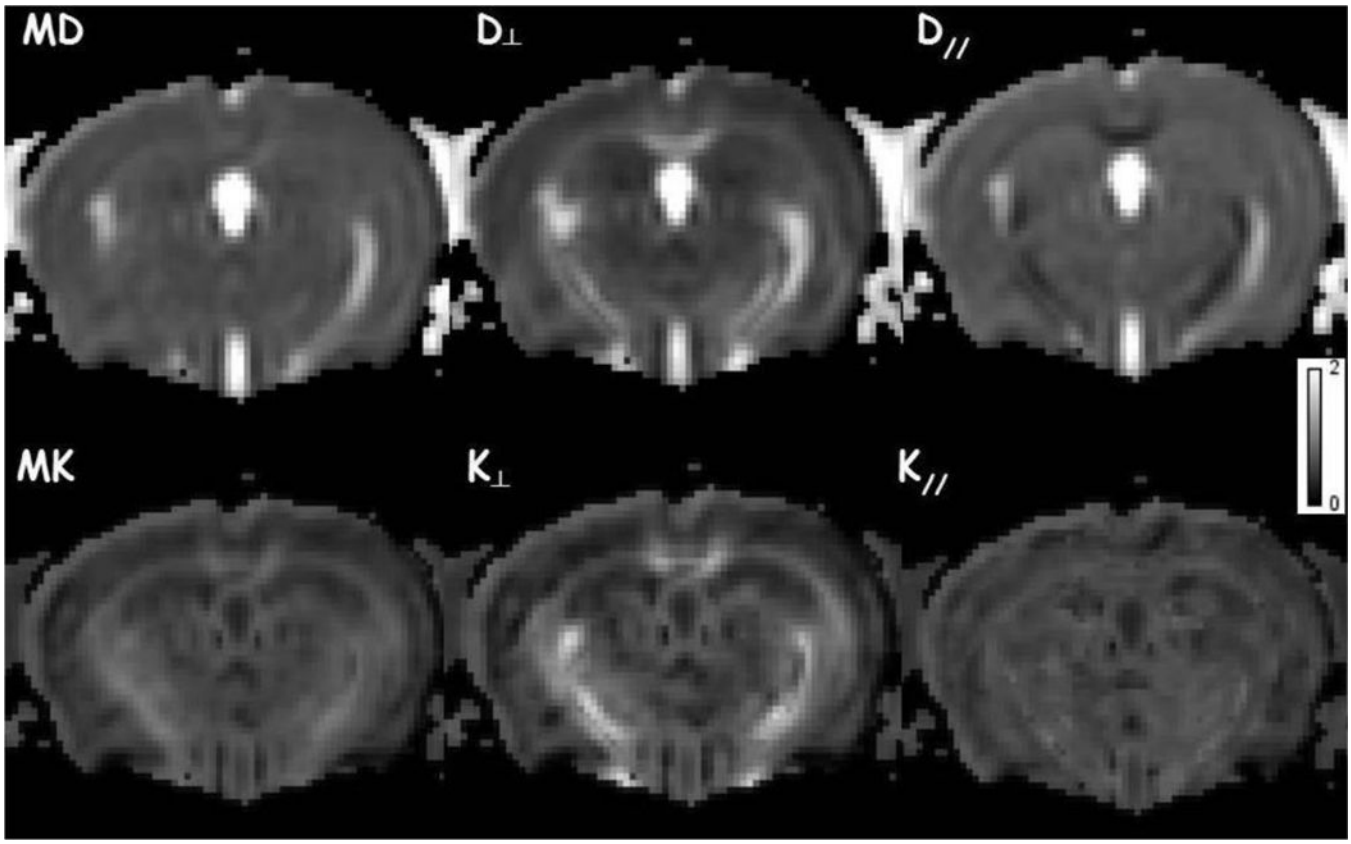

Figure 3.
Example of diffusion MRI parametric maps for a normossomic control (NS) mouse: mean (MD), axial ($D_{//}$) and radial ($D_{\perp}$) diffusivities; mean (MK), axial ($K_{//}$) and radial ($K_{\perp}$) kurtoses.

a

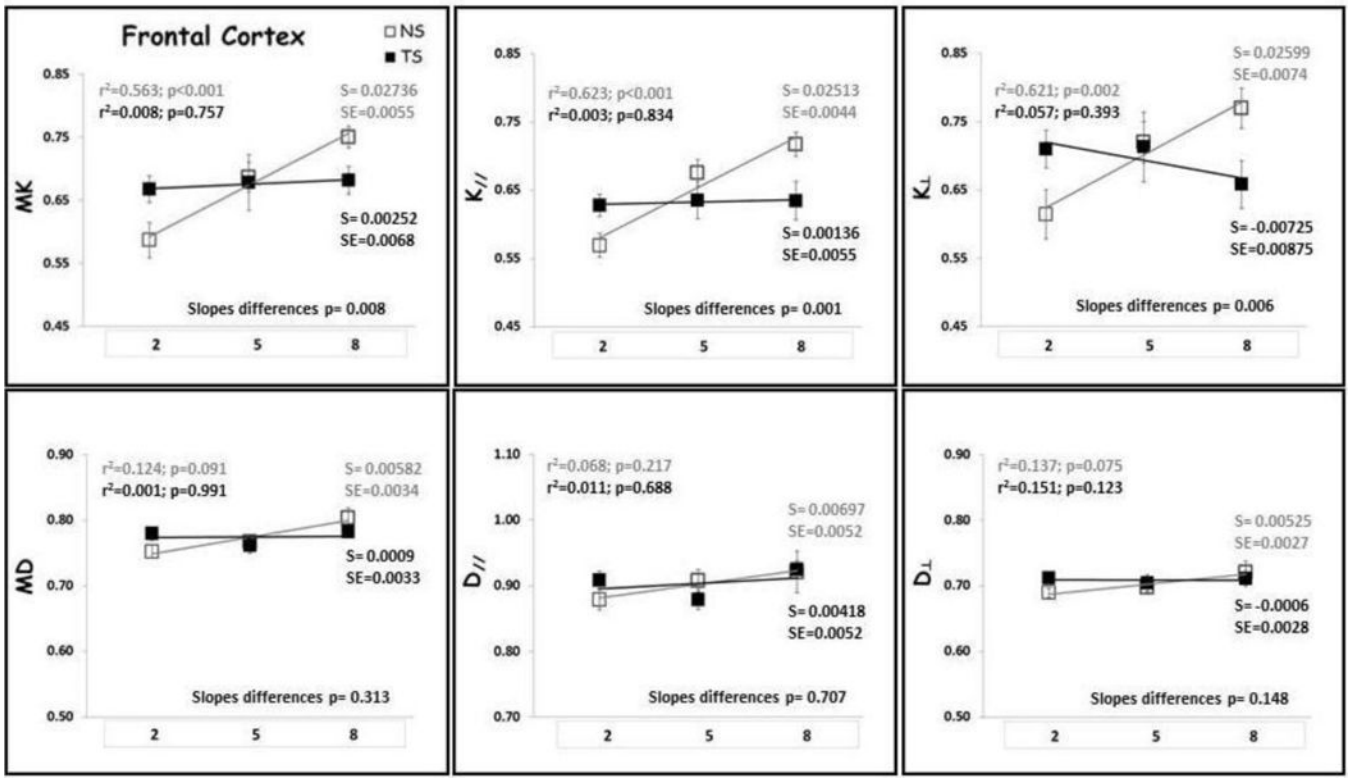

b

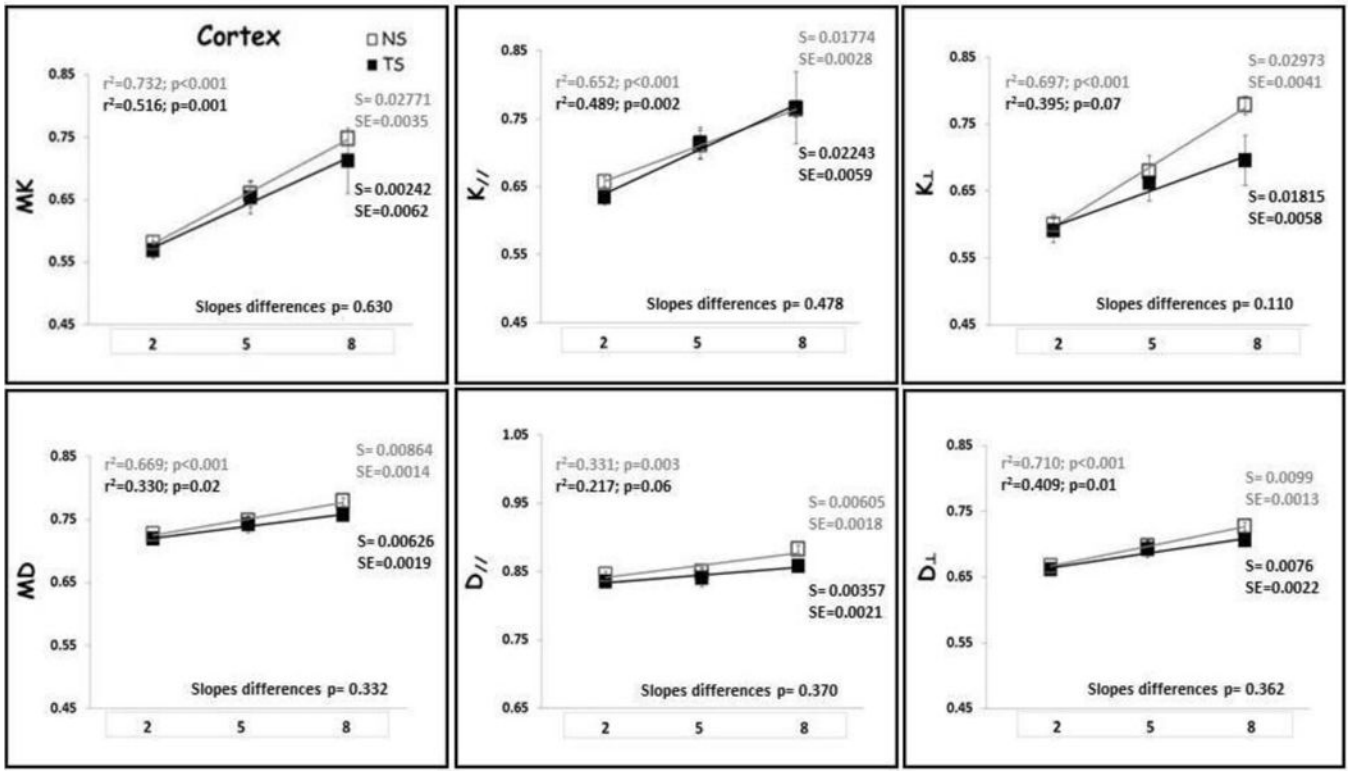

Figure 4.

(A) Frontal cortex (FC) and **(B)** Cortex (CT) DK and DT metrics means with age. TS mice are represented by black square, black regression line and black r^2 and slope values; NS mice are represented by gray square, gray regression line and gray r^2 and slope values. S= slope; SE= standard error of the slope. Mean diffusivity (MD); axial diffusivity ($D_{//}$); radial diffusivity ($D_{\perp}$); mean kurtosis (MK); axial kurtosis ($K_{//}$); radial kurtosis ($K_{\perp}$); months of age (2, 5 and 8).

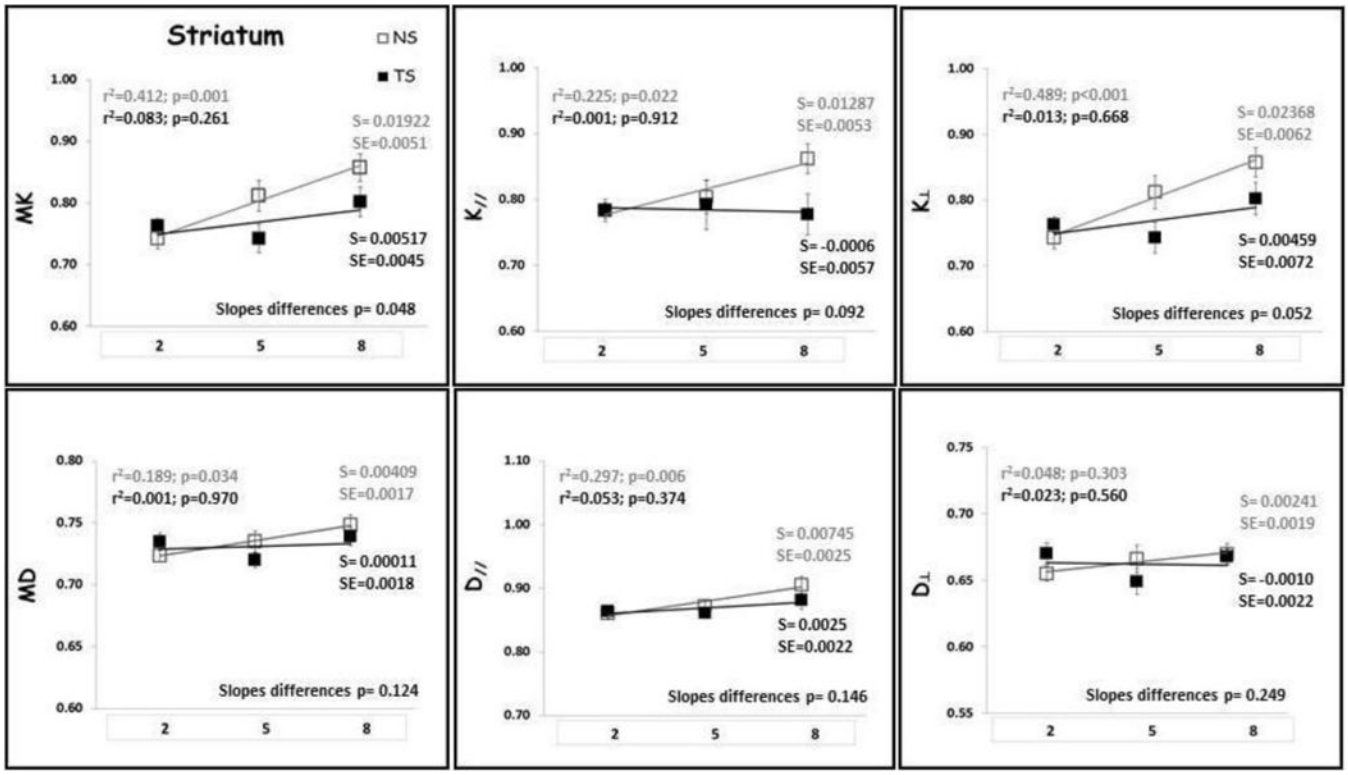

Figure 5.

Striatum (ST) DK and DT metrics means with age. TS mice are represented by black square, black regression line and black r^2 and slope values; NS mice are represented by gray square, gray regression line and gray r^2 and slope values. S= slope; SE= standard error of the slope. Mean diffusivity (MD); axial diffusivity ($D_{/\!/}$); radial diffusivity ($D_{\perp}$); mean kurtosis (MK); axial kurtosis ($K_{/\!/}$); radial kurtosis ($K_{\perp}$); months of age (2, 5 and 8).

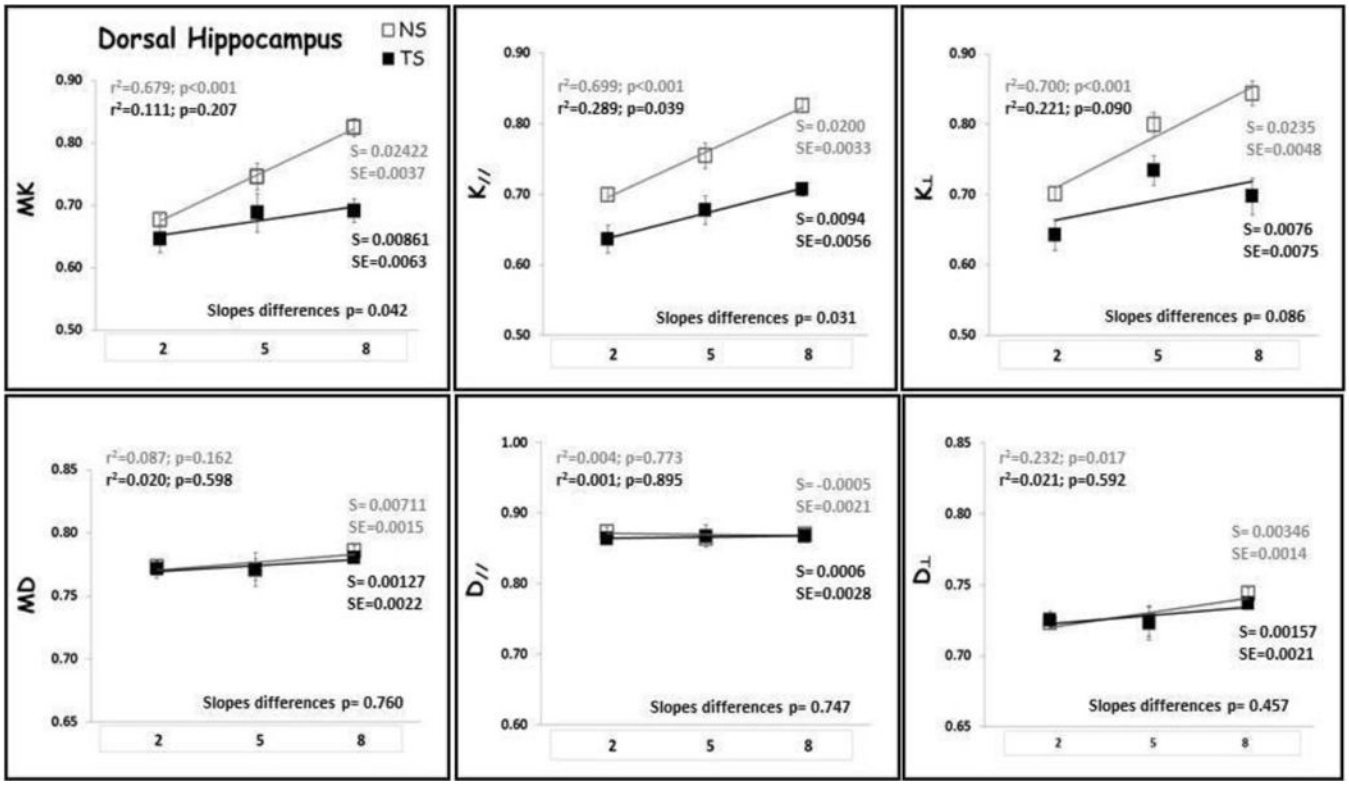

Figure 6.

Dorsal Hippocampus (HD) DK and DT metrics means with age. TS mice are represented by black square, black regression line and black r^2 and slope values; NS mice are represented by gray square, gray regression line and gray r^2 and slope values. S= slope; SE= standard error of the slope. Mean diffusivity (MD); axial diffusivity ($D_{//}$); radial diffusivity ($D_{\perp}$); mean kurtosis (MK); axial kurtosis ($K_{//}$); radial kurtosis ($K_{\perp}$); months of age (2, 5 and 8).

Table 1

Diffusion metrics estimates (mean ± standard error of the mean (SEM)) in each brain region of interest for the 2-month old mice.

		MD µm2/ms	$D_{//}$ µm2/ms	$D_{\perp}$ µm2/ms	MK	$K_{//}$	$K_{\perp}$
FC	NS	0.75 ± 0.03	0.88 ± 0.05	0.69 ± 0.02	0.60 ± 0.06	0.58 ± 0.04	0.62 ± 0.09
	TS	0.78 ± 0.03	0.91 ± 0.04	0.71 ± 0.02	0.67 ± 0.06	0.63 ± 0.05	0.71 ± 0.08
p-values		0.09	0.14	0.11	**0.03**	**0.03**	**0.05**
CT	NS	0.73 ± 0.01	0.85 ± 0.01	0.67 ± 0.01	0.58 ± 0.03	0.66 ± 0.02	0.60 ± 0.04
	TS	0.72 ± 0.01	0.84 ± 0.02	0.66 ± 0.01	0.57 ± 0.04	0.63 ± 0.03	0.59 ± 0.05
p-values		0.28	0.16	0.41	0.49	0.12	0.71
ST	NS	0.72 ± 0.02	0.86 ± 0.02	0.66 ± 0.02	0.74 ± 0.05	0.78 ± 0.05	0.83 ± 0.07
	TS	0.73± 0.02	0.86 ± 0.02	0.67 ± 0.02	0.76 ± 0.03	0.78 ± 0.04	0.84 ± 0.04
p-values		0.24	0.77	0.15	0.35	0.99	0.76
HT	NS	0.78 ± 0.01	0.87 ± 0.01	0.73 ± 0.01	0.67 ± 0.02	0.71 ± 0.02	0.66 ± 0.02
	TS	0.77 ± 0.01	0.87 ± 0.01	0.72 ± 0.01	0.65 ± 0.02	0.68 ± 0.02	0.66 ± 0.02
p-values		0.60	0.63	0.36	0.37	0.27	0.97
HD	NS	0.77 ± 0.01	0.87 ± 0.01	0.72 ± 0.01	0.68 ± 0.01	0.70 ± 0.01	0.70 ± 0.02
	TS	0.77 ± 0.01	0.86 ± 0.01	0.73 ± 0.01	0.63 ± 0.01	0.64 ± 0.02	0.64 ± 0.02
p-values		0.90	0.68	0.68	**0.04**	**0.01***	**0.02***
HV	NS	0.78 ± 0.01	0.87 ± 0.01	0.73 ± 0.01	0.66 ± 0.02	0.71 ± 0.02	0.64 ± 0.02
	TS	0.77 ± 0.01	0.86 ± 0.01	0.72 ± 0.01	0.65 ± 0.02	0.69 ± 0.02	0.66 ± 0.02
p-values		0.30	0.53	0.24	0.65	0.49	0.55

Diffusion metrics estimates (mean ± standard error of the mean (SEM)) in each brain region of interest for the 2 months old mice. *One-way ANOVA with significant p-values in bold; a (*) indicates that the group difference remained significant after applying Bonferroni correction*. Mean diffusivity (MD); axial diffusivity ($D_{//}$); radial diffusivity ($D_{\perp}$); mean kurtosis (MK); axial kurtosis ($K_{||}$); radial kurtosis ($K_{\perp}$); Ts65Dn (TS; *n*=8) and normossomic control (NS; *n*=8); frontal cortex (FC), cortex (CT), striatum (ST) and hippocampus (total – HT; dorsal – HD; ventral – HV).

Table 2

Diffusion metrics estimates (mean ± standard error of the mean (SEM)) in each brain region of interest for the 5-month old mice.

		MD	$D_{//}$	$D_{\perp}$	MK	$K_{//}$	$K_{\perp}$
		µm2/ms	µm2/ms	µm2/ms			
FC	NS	0.77 ± 0.03	0.91 ± 0.05	0.70 ± 0.03	0.69 ± 0.06	0.68 ± 0.05	0.72 ± 0.08
	TS	0.76 ± 0.03	0.88 ± 0.03	0.70 ± 0.03	0.68 ± 0.09	0.64 ± 0.05	0.71 ± 0.10
p-values		0.78	0.33	0.48	0.90	0.25	0.89
CT	NS	0.75 ± 0.02	0.85 ± 0.02	0.70 ± 0.02	0.66 ± 0.06	0.71 ± 0.04	0.68 ± 0.07
	TS	0.75 ± 0.03	0.84 ± 0.02	0.70 ± 0.03	0.65 ± 0.06	0.71 ± 0.05	0.66 ± 0.06
p-values		0.94	0.70	0.92	0.87	0.91	0.65
ST	NS	0.73 ± 0.02	0.87 ± 0.03	0.67 ± 0.03	0.83 ± 0.05	0.80 ± 0.08	0.95 ± 0.05
	TS	0.72 ± 0.01	0.86 ± 0.02	0.65 ± 0.02	0.74 ± 0.05	0.79 ± 0.08	0.80 ± 0.08
p-values		0.27	0.52	0.32	0.09	0.80	**0.001***
HT	NS	0.77 ± 0.01	0.86 ± 0.01	0.72 ± 0.01	0.72 ± 0.02	0.74 ± 0.02	0.72 ± 0.05
	TS	0.77 ± 0.01	0.89 ± 0.02	0.72 ± 0.01	0.72 ± 0.02	0.73 ± 0.04	0.68 ± 0.06
p-values		0.67	0.25	0.61	0.95	0.74	0.45
HD	NS	0.78 ± 0.01	0.87 ± 0.01	0.73 ± 0.01	0.75 ± 0.06	0.75 ± 0.05	0.80 ± 0.04
	TS	0.78 ± 0.01	0.88 ± 0.02	0.73 ± 0.01	0.69 ± 0.07	0.68 ± 0.04	0.73 ± 0.04
p-values		0.92	0.67	0.95	**0.04**	**0.03**	**0.04**
HV	NS	0.77 ± 0.02	0.86 ± 0.02	0.72 ± 0.01	0.71 ± 0.02	0.73 ± 0.02	0.71 ± 0.02
	TS	0.77 ± 0.01	0.90 ± 0.02	0.71 ± 0.01	0.70 ± 0.03	0.71 ± 0.03	0.70 ± 0.02
p-values		0.57	0.16	0.46	0.78	0.47	0.63

Diffusion metrics estimates (mean ± standard error of the mean (SEM)) in each brain region of interest for the 5 months old mice. *One-way ANOVA with significant p-values in bold; a (*) indicates that the group difference remained significant after applying Bonferroni correction*. Mean diffusivity (MD); axial diffusivity ($D_{//}$); radial diffusivity ($D_{\perp}$); mean kurtosis (MK); axial kurtosis ($K_{//}$); radial kurtosis ($K_{\perp}$); Ts65Dn (TS; *n*=5) and normossomic control (NS; *n*=8) groups; frontal cortex (FC), cortex (CT), striatum (ST) and hippocampus (total – HT; dorsal – HD; ventral – HV).

Table 3

Diffusion metrics estimates (mean ± standard error of the mean (SEM)) in each brain region of interest for the 8-month old mice.

		MD µm2/ms	$D_{//}$ µm2/ms	$D_{\perp}$ µm2/ms	MK	$K_{//}$	$K_{\perp}$
FC	NS	0.79 ± 0.06	0.92 ± 0.09	0.72 ± 0.05	0.75 ± 0.05	0.72 ± 0.04	0.75 ± 0.06
	TS	0.78 ± 0.02	0.92 ± 0.03	0.71 ± 0.02	0.68 ± 0.04	0.64 ± 0.05	0.66 ± 0.06
p-values		0.81	0.94	0.64	**0.04**	**0.03**	0.06
CT	NS	0.78 ± 0.02	0.88 ± 0.03	0.73 ± 0.02	0.75 ± 0.03	0.76 ± 0.03	0.78 ± 0.04
	TS	0.75 ± 0.01	0.86 ± 0.02	0.70 ± 0.02	0.72 ± 0.09	0.77 ± 0.09	0.70 ± 0.06
p-values		0.48	0.35	0.64	0.38	0.95	**0.03**
ST	NS	0.75 ± 0.02	0.91 ± 0.04	0.67 ± 0.02	0.86 ± 0.06	0.86 ± 0.05	0.97 ± 0.07
	TS	0.74 ± 0.02	0.88 ± 0.03	0.67 ± 0.01	0.80± 0.05	0.78 ± 0.06	0.86 ± 0.09
p-values		0.48	0.25	0.92	0.15	**0.03**	**0.04**
HT	NS	0.79 ± 0.01	0.88 ± 0.02	0.75 ± 0.01	0.81 ± 0.04	0.79 ± 0.02	0.83 ± 0.05
	TS	0.81 ± 0.02	0.90 ± 0.02	0.76 ± 0.01	0.71± 0.07	0.71 ± 0.10	0.71 ± 0.07
p-values		0.29	0.25	0.46	**0.02***	0.07	**0.01***
HD	NS	0.79 ± 0.01	0.87 ± 0.01	0.74 ± 0.01	0.82 ± 0.01	0.83 ± 0.01	0.85 ± 0.02
	TS	0.78 ± 0.01	0.87 ± 0.01	0.73 ± 0.00	0.69 ± 0.02	0.71 ± 0.02	0.70 ± 0.03
p-values		0.35	0.84	0.24	**0.001***	**0.001***	**0.002***
HV	NS	0.79 ± 0.01	0.88 ± 0.02	0.75 ± 0.01	0.80 ± 0.02	0.77 ± 0.03	0.82 ± 0.03
	TS	0.81 ± 0.02	0.91 ± 0.02	0.76 ± 0.02	0.71 ± 0.04	0.71 ± 0.04	0.71 ± 0.04
p-values		0.40	0.22	0.52	0.06	0.26	0.07

Diffusion metrics estimates (mean ± standard error of the mean (SEM)) in each brain region of interest for the 8 months old mice. *One-way ANOVA with significant p-values in bold; a (*) indicates that the group difference remained significant after applying Bonferroni correction*. Mean diffusivity (MD); axial diffusivity ($D_{//}$); radial diffusivity ($D_{\perp}$); mean kurtosis (MK); axial kurtosis ($K_{//}$); radial kurtosis ($K_{\perp}$); Ts65Dn (TS; *n*=4) and normossomic control (NS; *n*=8) groups; frontal cortex (FC), cortex (CT), striatum (ST) and hippocampus (total – HT; dorsal – HD; ventral – HV)